Determining Vibrational Solvation-Correlation Functions from Three-Pulse Infrared Photon Echoes†

A. Piryatinski and J. L. Skinner*

Theoretical Chemistry Institute and Department of Chemistry, University of Wisconsin, 1101 University Avenue, Madison, Wisconsin 53706

Received: January 28, 2002; In Final Form: May 14, 2002

Vibrational three-pulse photon echo experiments can probe ultrafast dynamics in condensed phase systems. The central objects of interest are vibrational frequency time-correlation functions, otherwise known as vibrational solvation-correlation functions. Established techniques for determining these correlation functions from experimental data include multiparameter nonlinear fits of the entire echo response, or peak-shift methods. In this paper we propose alternative approaches, closely related to those proposed recently for electronic echoes, involving the short-time slope of the echo intensity or amplitude. We explicitly consider the time-integrated intensity, the heterodyned and half-Fourier transformed amplitude, and the frequency-dispersed intensity. We describe approaches that can separately determine the solvation correlation function for the fundamental transition frequency fluctuations, and the cross-correlation function between the fundamental and excited-state frequency fluctuations. We illustrate the approaches with numerical calculations and also comment on the microscopic origin of frequency fluctuation correlations between different transitions.

I. Introduction

Solvation dynamics,[1−3] which refers to the relative motion of solute and solvent molecules in solution, plays an important role in a variety of processes such as electron transfer and chemical reactions. Optical spectroscopic techniques can provide an excellent probe of solvation dynamics because the solute's electronic transition frequency is very sensitive to relative solute−solvent positions and orientations. Changes in these positions and orientations as time evolves leads to a fluctuating (time-dependent) transition frequency, whose statistical properties can be measured (under different circumstances) by absorption spectroscopy, time-resolved fluorescence, transient hole burning, and three-pulse photon echoes.[1−10] These transition frequency fluctuations are most simply characterized by their two-point time-correlation function, which is called the solvation-correlation function (SCF). Much recent effort has been directed toward determining SCFs using time-resolved fluorescence, hole burning, and echoes, for systems where this dynamical information cannot be obtained from the absorption line shape because of inhomogeneous broadening.

In this paper we will focus on the three-pulse photon echo technique, which involves a sequence of three light pulses, separated by delay times t_1 and t_2. In the time-integrated version of the experiment (which we simply call the 3PE experiment), the total intensity is integrated for all times after the third pulse, rendering the signal a function of the two delay times t_1 and t_2. The most common method for extracting the SCF from the 3PE experiment is the three-pulse echo peak-shift (3PEPS) method,[9−12] which measures the position of the peak of the intensity along the t_1 axis as a function of t_2. It has been shown that for long times t_2 the peak position is proportional to the SCF (as a function of t_2).[11−13] Very recently Everitt, Geva, and Skinner (EGS) proposed a somewhat different method for extracting the SCF: they showed that the slope of the intensity in the t_1 direction at $t_1 = 0$ (which is still a function of t_2), normalized by its value at $t_2 = 0$, is equal to the normalized SCF for all times t_2.[13] As a more involved alternative to the above two methods, one can assume a functional form for the SCF, calculate the full t_1 and t_2 dependence of the signal directly, and then fit the parameters in the functional form by comparing to experiment.[14−17]

Quite recently the three-pulse photon echo technique has been extended into the infrared[17−37] and can therefore be used to study vibrational rather than electronic transitions. Whereas linear or nonlinear electronic spectroscopy can often be treated with a two-level model (because often only the ground-to-excited-state transition of interest is sufficiently near-resonant with the light), with vibrational spectroscopy this is often not the case. Labeling the ground, first excited, and second excited vibrational states of a particular vibrational mode on the solute by 0, 1, and 2, respectively, the 1−2 transition frequency is often near-resonant with the 0−1 transition, and so a third-order nonlinear experiment should usually be modeled with a three-level system. Recall that in the electronic case the transition frequency fluctuates in time due to molecular dynamics. The same is true in the case of vibrations, but now there are two fluctuating frequencies, corresponding to the 0−1 and 1−2 transitions. These two fluctuating frequencies are most simply characterized by three time-correlation functions, the vibrational solvation-correlation functions (VSCFs), involving the two frequencies each correlated with themselves, and their cross-correlation. Although there are theoretical reasons why these three VSCFs might be similar (see section V below), it would still be interesting to develop a scheme by which one could extract each one individually from experimental three-pulse echo data. As in the electronic case, the VSCFs provide information about intermolecular solute−solvent dynamics.

Although the time-integrated three-pulse echo technique described above is quite useful, more elaborate versions of the

† Part of the special issue "John C. Tully Festschrift".

* To whom correspondence should be addressed.

10.1021/jp0202542 CCC: $22.00
Published on Web 07/09/2002

three-pulse echo experiment contain even more information. For example, one can time-gate the intensity (T3PE) after the third pulse, one can send the signal after the third pulse through a monochromator to get a frequency-dispersed three-pulse echo (F3PE), or one can use heterodyne detection (H3PE) to time-resolve the electric field amplitude.[19,20,24,25,28,30,37,38] In this paper we show how one can extract two of the three VSCFs from three-pulse echo experiments, for each of the four versions, 3PE, T3PE, F3PE, and H3PE, discussed above. Our approaches are closely related to those developed earlier by EGS[13] in the case of electronic echoes, and (except in the case of T3PE) involve the short-time slope of intensities or amplitudes along the t_1 axis. We illustrate the approaches with numerical calculations, and we also comment on the microscopic origin of correlated frequency fluctuations for different transitions.

II. Vibrational Three-Pulse Echo Response Function

We consider a single anharmonic vibrational mode of the solute, which we treat quantum mechanically. We assume that all other nuclear dynamics of the solute/solvent system can be treated classically. Within this picture the interaction between the anharmonic oscillator and the "bath" (all other nuclear degrees of freedom) leads to fluctuating (time-dependent) energy levels of the anharmonic oscillator. In what follows we will only need to consider the first three levels of the oscillator; the appropriate three-level Hamiltonian is therefore

$$H_0(t) = \sum_{n=0}^{2} \hbar(\omega_n + \delta\omega_n(t))|n\rangle\langle n| \qquad (1)$$

where $\hbar\omega_n$ is the mean energy of the nth level, $\hbar\delta\omega_n(t)$ are the time-dependent fluctuations from the mean, and $|n\rangle$ are the eigenstates of the oscillator. Note that because the above Hamiltonian is diagonal in these eigenstates, it will not lead to any population relaxation processes, and hence we do not consider such processes in what follows.

Including the interaction with a time-dependent electric field, the total Hamiltonian is

$$H(t) = H_0(t) - \mu E(t) \qquad (2)$$

where μ is the projection of the vector dipole operator in the direction of the vector electric field, and $E(t)$ is the field amplitude. Here we will not consider rotational dynamics of the solute, and so μ is time independent.

Within such a model the normalized linear absorption line shape for the fundamental (0−1) transition is[6,7,38]

$$I(\Omega) = \frac{1}{2\pi}\int_{-\infty}^{\infty} dt\, e^{i(\Omega-\omega_{10})t}\langle \exp[-i\int_0^t \delta\omega_{10}(\tau)\, d\tau]\rangle \qquad (3)$$

where $\omega_{10} = \omega_1 - \omega_0$ and $\delta\omega_{10}(t) = \delta\omega_1(t) - \delta\omega_0(t)$. The angular brackets indicate a classical equilibrium statistical mechanical average.

Our primary interest is in the nonlinear response of the oscillator following excitation by a sequence of three nonoverlapping IR pulses, as shown in Figure 1A, whose total electric field is $E(t) = \sum_{n=1}^{3} \mathcal{E}_n(t - \tau_n)\exp\{i(\mathbf{k}_n\cdot\mathbf{r} - \omega t)\} + \text{cc}$. The nth pulse is characterized by the pulse envelope $\mathcal{E}_n(t)$, interaction time τ_n, wavevector $\mathbf{k}_n$, and central frequency ω. Because the oscillator's fundamental transition energy is assumed to be much greater than kT, just before the first pulse the oscillator is in its ground vibrational state. We calculate the polarization of the system at time t (which is after the last pulse has interacted with the system), from $P(t) = \langle \text{Tr}[\mu\rho(t)]\rangle$. $\rho(t)$ is the time-dependent density operator for the three-level system. The polarization has components with several different wavevectors; here we are interested in the photon echo phase matching conditions described by the wavevector $\mathbf{k}_s = \mathbf{k}_3 + \mathbf{k}_2 - \mathbf{k}_1$. For this component we can write $P(t) \sim e^{i\mathbf{k}_s\cdot\mathbf{r}}R(t_3,t_2,t_1) + \text{cc}$, where $R(t_3,t_2,t_1)$ is the nonlinear response function. As shown, it depends on the time differences $t_1 = \tau_2 - \tau_1$, $t_2 = \tau_3 - \tau_2$, and $t_3 = t - \tau_3$ (see Figure 1A). When the interaction with each pulse is taken to first order in perturbation theory, in the limit of delta-function pulse envelopes, the response function is[13,21,38]

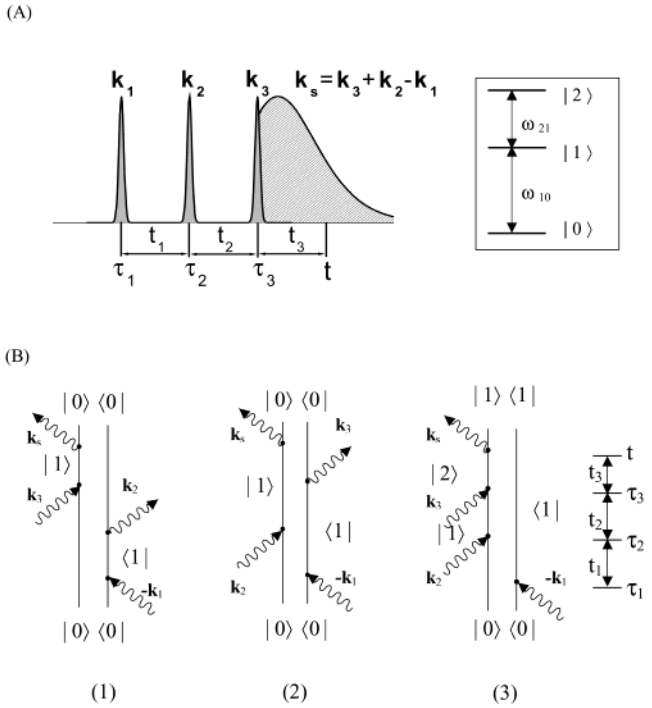

Figure 1. (A) Schematic diagram of three-pulse echo pulse sequence and signal generated in the direction $\mathbf{k}_s = \mathbf{k}_3 + \mathbf{k}_2 - \mathbf{k}_1$. Also shown is the level scheme. (B) Double-sided Feynman diagrams describing all contributions to the three-pulse echo signal for the three-level system in the rotating wave approximation.

$$R(t_3,t_2,t_1) = i^3\{\langle \exp[i\int_0^{t_1}\delta\omega_{10}(\tau)\, d\tau - i\int_{t_1+t_2}^{t_1+t_2+t_3}\delta\omega_{10}(\tau)\, d\tau]\rangle e^{-i\omega_{10}t_3} - (\kappa^2/2)\langle \exp[i\int_0^{t_1}\delta\omega_{10}(\tau)\, d\tau - i\int_{t_1+t_2}^{t_1+t_2+t_3}\delta\omega_{21}(\tau)\, d\tau]\rangle e^{-i\omega_{21}t_3}\} \qquad (4)$$

In the above $\omega_{21} = \omega_2 - \omega_1$, $\delta\omega_{21}(t) = \delta\omega_2(t) - \delta\omega_1(t)$, and $\kappa = \mu_{21}/\mu_{10}$, where μ_{21} and μ_{10} are the matrix elements of the dipole operator μ. Note that we have not explicitly shown all overall phase factors; in particular, sometimes others include $e^{i\omega_{10}t_1}$.[17] For heterodyned experiments, the absolute phase of the response function must be determined experimentally.[20]

This response function is the result of the interference among three Liouville-space pathways described by the Feynman diagrams in Figure 1B.[38] Diagrams 1 and 2 involve only 0−1 coherences propagating during t_1 and t_3. In our semiclassical model these diagrams lead to identical contributions, and their sum is the first term in the above. Diagram 3 involves the 0−1 coherence propagating during t_1 as well as the 1−2 coherence propagating during t_3. It corresponds to the second term above. If the oscillator were harmonic, then $\omega_{21} = \omega_{10}$ and $\kappa^2 = 2$. If in addition $\delta\omega_{21}(t) = \delta\omega_{10}(t)$ (see section V), as is well-known, the third-order response vanishes.[17]

We next define the three (classical) VSCFs

$$C_1(t) = \langle \delta\omega_{10}(t)\, \delta\omega_{10}(0)\rangle$$
$$C_2(t) = \langle \delta\omega_{10}(t)\, \delta\omega_{21}(0)\rangle$$
$$C_3(t) = \langle \delta\omega_{21}(t)\, \delta\omega_{21}(0)\rangle \quad (5)$$

It is often the case that the frequency fluctuations $\delta\omega_{10}(t)$ and $\delta\omega_{21}(t)$ are approximately Gaussian. If they are, then the statistics of the fluctuations are described completely by these two-point time-correlation functions, and moreover, the cumulant expansions for the averages of the relevant exponentials in the above truncate exactly at second order, giving rise to[13,21,38]

$$R(t_3,t_2,t_1) = i^3\Big\{\exp[f_1(t_1,t_2,t_3) - i\omega_{10}t_3] - \frac{\kappa^2}{2}\exp[f_2(t_1,t_2,t_3) - i\omega_{21}t_3]\Big\} \quad (6)$$

where

$$f_1(t_1,t_2,t_3) = -g_1(t_1) + g_1(t_2) - g_1(t_3) - g_1(t_1+t_2) - g_1(t_2+t_3) + g_1(t_1+t_2+t_3)$$
$$f_2(t_1,t_2,t_3) = -g_1(t_1) + g_2(t_2) - g_3(t_3) - g_2(t_1+t_2) - g_2(t_2+t_3) + g_2(t_1+t_2+t_3) \quad (7)$$

These two functions are real, because each contains linear combinations of the "line-shape" functions

$$g_n(t) = \int_0^t dt' \int_0^{t'} dt''\, C_n(t'') = \int_0^t dt'\, (t-t')C_n(t') \qquad n = 1-3 \quad (8)$$

which are real in the case of a classical bath. We note that $f_2(t_1,t_2,t_3)$ contains all three line-shape functions, whereas $f_1(t_1,t_2,t_3)$ depends only on $g_1(t)$. Under the same conditions as above the expression for the absorption line shape (eq 3) becomes[6,7,38]

$$I(\Omega) = \frac{1}{2\pi}\int_{-\infty}^{\infty} dt\, e^{i(\Omega-\omega_{10})t}\exp[-g_1(t)] \quad (9)$$

III. Determining the Vibrational Solvation-Correlation Functions

The main goal of this paper is to propose methods for determining the VSCFs from vibrational three-pulse photon echo experiments. To this end we consider four detection schemes.[28] The first is the time-integrated intensity

$$I(t_2,t_1) = \int_0^{\infty} dt_3\, |R(t_3,t_2,t_1)|^2 \quad (10)$$

which, as discussed in the Introduction, we simply call the 3PE intensity. In the second scheme one measures the time-gated intensity (T3PE), given by

$$I(t_3,t_2,t_1) = |R(t_3,t_2,t_1)|^2 \quad (11)$$

In the third scheme one uses heterodyne detection (H3PE) to measure the (complex) amplitude $R(t_3,t_2,t_1)$ directly. One can equally well represent this amplitude by its half-Fourier transform (in t_3):

$$\tilde{R}(\Omega,t_2,t_1) = \int_0^{\infty} dt_3\, R(t_3,t_2,t_1)\exp(i\Omega t_3) \quad (12)$$

In the fourth scheme the signal is sent through a monochromator, yielding the frequency-dispersed (F3PE) intensity, given by

$$I(\Omega,t_2,t_1) = |\tilde{R}(\Omega,t_2,t_1)|^2 \quad (13)$$

For a given specification of the fluctuating anharmonic oscillator, some of the detection schemes will be more useful than others in determining VSCFs, and so in what follows we will focus on a number of special cases. In this context it is important to consider the relative magnitudes of three quantities: the laser bandwidth, the anharmonicity (defined by $\Delta = \omega_{10} - \omega_{21}$), and the absorption line width. If the anharmonicity is larger than the line width, the ω_{10} and ω_{21} resonances will be spectrally separated. If in addition the laser bandwidth is smaller than the anharmonicity, the 1−2 transition will not be excited. In this limit one can simply neglect the second term in eq 6, which we will call the two-level approximation. Another important special circumstance is when the VSCFs are all identical. As discussed in section V, when the anharmonicity is sufficiently weak, $\delta\omega_{21}(t) \simeq \delta\omega_{10}(t)$, which indeed renders the three VSCFs the same. In this weak anharmonicity limit we will also generally assume that the ratio of the relevant dipole matrix elements (μ_{21}/μ_{10}) is given adequately by its harmonic value. Below we consider specific combinations of these special cases and detection schemes that are useful in determining VSCFs.

A. Time-Integrated Intensity, Two-Level Approximation. First consider the situation when the anharmonicity is sufficiently large and the laser bandwidth is sufficiently small that we can neglect the second term in eq 6. In this case the response function involves only $g_1(t)$ and hence $C_1(t)$. This reduces precisely to the two-level situation considered by others,[11,12] including EGS,[13] within the context of electronic spectroscopy. EGS considered the initial slope of the (integrated) 3PE signal in the t_1 direction, defined by

$$S(t_2) = \left[\frac{\partial I(t_2,t_1)}{\partial t_1}\right]_{t_1=0} \quad (14)$$

From eqs 6, 7, and 10 this gives

$$S(t_2) = 2\int_0^{\infty} dt_3\, [\dot{g}_1(t_2+t_3) - \dot{g}_1(t_2)]e^{-2g_1(t_3)} \quad (15)$$

The VSCFs $C_n(t)$ are characterized by their initial values $C_n(0) \equiv \sigma_n^2$, and correlation times $\tau_n \equiv \int_0^{\infty} dt\, C_n(t)/C_n(0)$. The dimensionless product $\sigma_1\tau_1$ determines whether the line shape for the fundamental transition is inhomogeneous, is homogeneous, or is in the intermediate modulation regime.[6,39] If $\sigma_1\tau_1 \gg 1$, the system is inhomogeneously broadened. In the electronic[13] case we found that in this limit it was useful to expand our echo formulas in powers of t_3. Thus, for example, to lowest order $g_1(t_3) = \sigma_1^2\, t_3^2/2$. Because this appears in the exponent in eq 15, it will effectively cut off the integrand for $t_3 \gg 1/\sigma_1$. Expanding the rest of the integrand to lowest order in t_3 (and using eq 8) then gives

$$S(t_2) = 2C_1(t_2)\int_0^{\infty} dt_3\, t_3 e^{-\sigma_1^2 t_3^2} \quad (16)$$

From this we see immediately that

$$\bar{C}_1(t_2) = S(t_2)/S(0) \quad (17)$$

where $\bar{C}_n(t) = C_n(t)/C_n(0)$ are the normalized VSCFs. Thus we see that the ratio of the slope at time t_2 to its initial value is

precisely the normalized solvation-correlation function, as it was in the case of electronic echoes.[13]

To make the connection to previous work of others related to the 3PEPS approach,[11,12] we define the peak shift $t_1^*(t_2)$ by

$$\left[\frac{\partial I(t_2,t_1)}{\partial t_1}\right]_{t_1=t_1^*(t_2)} = 0 \tag{18}$$

To derive an expression for the peak shift in the inhomogeneous limit, we expand $f_1(t_1,t_2,t_3)$ in powers of t_3 and t_1, to obtain[13]

$$f_1(t_1,t_2,t_3) \simeq -\frac{{\sigma_1}^2}{2}[{t_1}^2 + {t_3}^2 - 2t_1t_3\bar{C}_1(t_2)] \tag{19}$$

Substituting this into eqs 6 and 10, and using the definition of the peak shift, then gives

$$\int_0^\infty \mathrm{d}t_3\,[t_1^*(t_2) - t_3\bar{C}_1(t_2)] \times \exp\{-{\sigma_1}^2[{t_3}^2 - 2t_1^*(t_2)t_3\bar{C}_1(t_2)]\} = 0 \tag{20}$$

For long enough times t_2 such that $\bar{C}_1(t_2) \ll 1$, one can neglect the second term in the above exponential, leading directly to the simple result that

$$\bar{C}_1(t_2) = t_1^*(t_2)/T_\mathrm{p} \tag{21}$$

with $T_\mathrm{p} = 1/\sqrt{\pi}\sigma_1$. Thus this recovers the result of others[11,12] that for sufficiently long times the peak shift is proportional to the solvation-correlation function. As we discussed earlier, the slope method has the advantage over the 3PEPS approach in that one can obtain the solvation-correlation function for *all* times, although it has the possible disadvantage that pulse-overlap effects may complicate the determination of the initial slope.[13,40,41]

In electronic spectroscopy, line shapes are indeed often inhomogeneously broadened. In vibrational spectroscopy, however, this is less likely to be the case, because the rms frequency fluctuations σ_1 will typically be somewhat smaller, whereas the correlation time τ_1 remains comparable. Therefore it is of interest to develop corrections to eq 17, which will lead to improved results when the system is not in the inhomogeneous limit. To this end one keeps the next-order term in the expansion of $\dot{g}_1(t_2 + t_3)$ in eq 15. Using the fact that $C_1(t)$ is even in time, and so $\dot{C}_1(0) = 0$, this gives

$$\bar{C}_1(t_2) + T_1\ddot{\bar{C}}_1(t_2) = S(t_2)/S(0) \tag{22}$$

where $T_1 = \sqrt{\pi}/4\sigma_1$. Note that T_1 goes to zero as σ_1 gets large (the inhomogeneous limit), recovering eq 17. Equation 22 can be integrated to yield

$$\bar{C}_1(t_2) = \mathrm{e}^{-t_2/T_1}\left(1 + \frac{1}{T_1}\int_0^{t_2}\mathrm{d}\tau\,\mathrm{e}^{\tau/T_1}[S(\tau)/S(0)]\right) \tag{23}$$

Because ${\sigma_1}^2$ is the variance of the line shape (even when the system is not in the inhomogeneous limit), one can easily determine it experimentally and then calculate T_1, which with the above will lead to an improved determination of $\bar{C}_1(t_2)$ when the system is not in the inhomogeneous limit.

B. Time-Gated Intensity, Two-Level Approximation. The time-gated intensity (see eq 11) is simply the squared magnitude of the complex amplitude $R(t_3,t_2,t_1)$, which can be measured with or without heterodyne detection. In the small bandwidth and large anharmonicity limit we again can make the two-level approximation and keep only the first term in eq 6. In the inhomogeneous limit $f_1(t_1,t_2,t_3)$ is given approximately by eq 19. The "diagonal" time-gated intensity is simply $I(t_1,t_2,t_1)$. The above then leads directly to

$$I(t_1,t_2,t_1) = \exp\{-2{\sigma_1}^2\,{t_1}^2[1 - \bar{C}_1(t_2)]\} \tag{24}$$

From this expression it would be a simple matter to extract $\bar{C}_1(t_2)$, as in the case of electronic echoes.[13]

C. Time-Integrated Intensity, Identical VSCFs. When not in the small bandwidth/large anharmonicity limit, both resonances are excited and one must now keep both terms in eq 6. But if the anharmonicity is weak enough, the VSCFs are identical, and $f_2(t_1,t_2,t_3) = f_1(t_1,t_2,t_3)$. In addition we take $\kappa^2 = 2$. In this case eq 6 becomes[17]

$$R(t_3,t_2,t_1) = i^3\mathrm{e}^{-i\omega_{10}t_3}\mathrm{e}^{f_1(t_1,t_2,t_3)}[1 - \mathrm{e}^{i\Delta t_3}] \tag{25}$$

Note again that if the mode is strictly harmonic, so $\Delta = 0$, the response function vanishes completely.[17]

As in section III.A we define the slope by eq 14, and in this case it is given by

$$S(t_2) = 8\int_0^\infty \mathrm{d}t_3\,\sin^2(\Delta t_3/2)[\dot{g}_1(t_2+t_3) - \dot{g}_1(t_2)]\mathrm{e}^{-2g_1(t_3)} \tag{26}$$

Making the same approximations, valid in the inhomogeneous limit, as in section III.A, we find that

$$S(t_2) = 8C_1(t_2)\int_0^\infty \mathrm{d}t_3\,t_3\,\sin^2(\Delta t_3/2)\mathrm{e}^{-{\sigma_1}^2{t_3}^2} \tag{27}$$

From this, one again sees that eq 17 follows immediately.

In this case we can also develop corrections to the inhomogeneous limit. As in section III.A we find that eqs 22 and 23 are valid, but now

$$T_1 = \frac{\sqrt{\pi}}{4\sigma_1}\frac{[1 - (1 - {\zeta_1}^2/2)\mathrm{e}^{-{\zeta_1}^2/4}]}{\zeta_1 D(\zeta_1/2)} \tag{28}$$

where $\zeta_1 = \Delta/\sigma_1$ and $D(z)$ is Dawson's integral: $D(z) = \mathrm{e}^{-z^2}\int_0^z \mathrm{d}x\,\mathrm{e}^{x^2}$. The definite integrals necessary to derive this result are evaluated in the Appendix. Because this subsection involves weak anharmonicity, in most cases it is probably safe to take the limit $\zeta_1 \to 0$, which leads to the simpler result $T_1 = 3\sqrt{\pi}/8\sigma_1$.

We can again derive a long-time relationship between the peak shift and the VSCF from the definition of eq 18. Again using eq 19, valid in the inhomogeneous limit, we find that

$$\int_0^\infty \mathrm{d}t_3\,[t_1^*(t_2) - t_3\bar{C}_1(t_2)]\,\sin^2(\Delta t_3/2)\mathrm{e}^{-{\sigma_1}^2{t_3}^2} = 0 \tag{29}$$

As before this leads to the simple result of eq 21, except for now

$$T_\mathrm{p} = \frac{1}{\sqrt{\pi}\sigma_1}\frac{\zeta_1 D(\zeta_1/2)}{(1 - \mathrm{e}^{-{\zeta_1}^2/4})} \tag{30}$$

For details the reader is again referred to the Appendix. In the limit $\zeta_1 \to 0$ we get the simpler result $T_\mathrm{p} = 2/\sqrt{\pi}\sigma_1$.

D. Time-Gated Intensity, Identical VSCFs. Using eqs 11, 19, and 25, we can write the diagonal time-gated intensity as

$$I(t_1,t_2,t_1) = 4\,\sin^2(\Delta t_1/2)\,\exp\{-2{\sigma_1}^2\,{t_1}^2[1 - \bar{C}_1(t_2)]\} \tag{31}$$

Knowing both Δ and σ_1 would allow one to determine $\bar{C}_1(t_2)$ in a straightforward manner.

E. Heterodyned Amplitude. As in section III.C, when not in the small bandwidth/strong anharmonicity limit, both terms in eq 6 must be included. But if the anharmonicity is not sufficiently weak, the three VSCFs are in general different (see section V), and so $f_1(t_1,t_2,t_3)$ differs from $f_2(t_1,t_2,t_3)$. In this case the situation is more complicated, and it appears difficult to arrive at simple ways to determine the different VSCFs from the integrated intensity. However, we can turn to the half-Fourier transformed heterodyned amplitude as in eq 12. We can first isolate the two functions $f_1(t_1,t_2,t_3)$ and $f_2(t_1,t_2,t_3)$ by noticing that

$$\tilde{R}_r(\omega_{10},t_2,t_1) = -\frac{\kappa^2}{2}\int_0^\infty dt_3 \exp[f_2(t_1,t_2,t_3)] \sin(\Delta t_3)$$

$$\tilde{R}_r(\omega_{21},t_2,t_1) = -\int_0^\infty dt_3 \exp[f_1(t_1,t_2,t_3)] \sin(\Delta t_3) \quad (32)$$

where $\tilde{R}_r(\Omega,t_2,t_1)$ is the real part of $\tilde{R}(\Omega,t_2,t_1)$. Thus by evaluating the Fourier transformed amplitude at the two different resonances, one can discriminate between the Liouville-space pathways represented by diagrams 1 and 2, and by diagram 3, even if the resonances are not spectrally separated!

We again introduce the slope at $t_1 = 0$ by

$$S(\Omega,t_2) = \left[\frac{\partial \tilde{R}_r(\Omega,t_2,t_1)}{\partial t_1}\right]_{t_1=0} \quad (33)$$

From this definition we then have

$$S(\omega_{10},t_2) = -\frac{\kappa^2}{2}\int_0^\infty dt_3 \sin(\Delta t_3)[\dot{g}_2(t_2+t_3) - \dot{g}_2(t_2)]e^{-g_3(t_3)} \quad (34)$$

$$S(\omega_{21},t_2) = -\int_0^\infty dt_3 \sin(\Delta t_3)[\dot{g}_1(t_2+t_3) - \dot{g}_1(t_2)]e^{-g_3(t_3)} \quad (35)$$

As in sections III.A and III.C we expand in powers of t_3, which leads to

$$\bar{C}_1(t_2) = e^{-t_2/T_1}\left(1 + \frac{1}{T_1}\int_0^{t_2} d\tau\, e^{\tau/T_1}[S(\omega_{21},\tau)/S(\omega_{21},0)]\right) \quad (36)$$

$$\bar{C}_2(t_2) = e^{-t_2/T_2}\left(1 + \frac{1}{T_2}\int_0^{t_2} d\tau\, e^{\tau/T_2}[S(\omega_{10},\tau)/S(\omega_{10},0)]\right) \quad (37)$$

The times T_1 and T_2 can be shown (see the Appendix) to be

$$T_1 = \frac{e^{\zeta_1^2/2}}{2\sqrt{\pi}\sigma_1\zeta_1}[\sqrt{2}\zeta_1 + 2(1-\zeta_1^2)D(\zeta_1/\sqrt{2})] \quad (38)$$

$$T_2 = \frac{e^{\zeta_3^2/2}}{2\sqrt{\pi}\sigma_3\zeta_3}[\sqrt{2}\zeta_3 + 2(1-\zeta_3^2)D(\zeta_3/\sqrt{2})] \quad (39)$$

In the above $\zeta_3 = \Delta/\sigma_3$. In the inhomogeneous limit both of these times go to zero, and similar to before

$$\bar{C}_1(t_2) = \frac{S(\omega_{21},t_2)}{S(\omega_{21},0)}$$

$$\bar{C}_2(t_2) = \frac{S(\omega_{10},t_2)}{S(\omega_{10},0)} \quad (40)$$

In summary, the heterodyned approach allows one to determine independently the normalized VSCF for the fundamental transition, and the normalized VSCF involving the cross-correlation between the two transitions.

For completeness we can define a peak shift in this case by

$$\left[\frac{\partial \tilde{R}_r(\Omega,t_2,t_1)}{\partial t_1}\right]_{t_1=t_1^*(\Omega,t_2)} = 0 \quad (41)$$

As in previous sections one can show that for long times t_2 the VSCFs are proportional to the peak shifts. In this case

$$\bar{C}_1(t_2) = t_1^*(\omega_{21},t_2)/T_{1p} \quad (42)$$

$$\bar{C}_2(t_2) = t_1^*(\omega_{10},t_2)/T_{2p} \quad (43)$$

and the times are given by

$$T_{1p} = \frac{\sqrt{\pi}\zeta_1 e^{-\zeta_1^2/2}}{2\sigma_1 D(\zeta_1/\sqrt{2})} \quad (44)$$

$$T_{2p} = \frac{\sqrt{\pi}\sigma_2^2\zeta_3 e^{-\zeta_3^2/2}}{2\sigma_1^2\sigma_3 D(\zeta_3/\sqrt{2})} \quad (45)$$

F. Frequency-Dispersed Intensity, Separated Resonances. The last detection scheme considered herein involves the frequency-dispersed intensity eq 13, which is particularly useful if the two resonances are spectrally separated. This occurs when $\Delta \gg \sigma_1, \sigma_3$. The integrand of $\tilde{R}(\Omega,t_2,t_1)$ in eq 12 has two terms (as long as one is not in the small bandwidth limit), oscillating at two different frequencies. For $\Omega = \omega_{10}$ the first term does not oscillate, but the second term does so with frequency Δ. These fast oscillations will kill the second term relative to the first, and so to a good approximation

$$I(\omega_{10},t_2,t_1) = \left(\int_0^\infty dt_3 \exp[f_1(t_1,t_2,t_3)]\right)^2 \quad (46)$$

Likewise

$$I(\omega_{21},t_2,t_1) = \frac{\kappa^2}{4}\left(\int_0^\infty dt_3 \exp[f_2(t_1,t_2,t_3)]\right)^2 \quad (47)$$

We again define the slope at $t_1 = 0$, in this case by

$$S(\Omega,t_2) = \left[\frac{\partial I(\Omega,t_2,t_1)}{\partial t_1}\right]_{t_1=0} \quad (48)$$

Making approximations valid near the inhomogeneous limit in this case then leads to

$$\bar{C}_1(t_2) = e^{-t_2/T_1}\left(1 + \frac{1}{T_1}\int_0^{t_2} d\tau\, e^{\tau/T_1}[S(\omega_{10},\tau)/S(\omega_{10},0)]\right) \quad (49)$$

$$\bar{C}_2(t_2) = e^{-t_2/T_2}\left(1 + \frac{1}{T_2}\int_0^{t_2} d\tau\, e^{\tau/T_2}[S(\omega_{21},\tau)/S(\omega_{21},0)]\right) \quad (50)$$

The times T_1 and T_2 are $T_1 = \sqrt{\pi}/2\sqrt{2}\sigma_1$, and $T_2 = \sqrt{\pi}/2\sqrt{2}\sigma_3$. In the inhomogeneous limit both of these times go to zero, and similar to before

$$\bar{C}_1(t_2) = \frac{S(\omega_{10},t_2)}{S(\omega_{10},0)}$$

$$\bar{C}_2(t_2) = \frac{S(\omega_{21},t_2)}{S(\omega_{21},0)} \tag{51}$$

Note that the above equations differ from those in section III.E in that the resonances are reversed!

For completeness we can define a peak shift in this case by

$$\left[\frac{\partial I(\Omega,t_2,t_1)}{\partial t_1}\right]_{t_1=t_1^*(\Omega,t_2)} = 0 \tag{52}$$

As in previous sections one can show that for long times t_2 the VSCFs are proportional to the peak shifts. In this case

$$\bar{C}_1(t_2) = t_1^*(\omega_{10},t_2)/T_{1p} \tag{53}$$

$$\bar{C}_2(t_2) = t_1^*(\omega_{21},t_2)/T_{2p} \tag{54}$$

and the times are given by $T_{1p} = \sqrt{2}/\sqrt{\pi}\sigma_1$ and $T_{2p} = \sqrt{2}\sigma_2^2/\sqrt{\pi}\sigma_1^2\sigma_3$.

In summary, then, if the system is in the inhomogeneous limit, one can easily relate the slope of the various quantities defined above at $t_1 = 0$ to two of the three normalized VSCFs. If the system is not too far from the inhomogeneous limit, then equations like, for example, eq 23, can still be used to obtain the VSCFs.

IV. Model Calculations

To illustrate the proposed techniques, and especially to see how accurate the zeroth- and first-order approaches for obtaining the VSCFs from the slopes are as one moves away from the inhomogeneous limit, in this section we present some numerical results corresponding to the cases discussed in sections III.C, III.E, and III.F. (Results for the two-level model discussed in section III.A were presented earlier in the context of electronic echoes by EGS.[13]) To this end we consider a simple phenomenological model for the three VSCFs:

$$C_n(t) = \frac{\sigma_n^2 \cosh(b_n t)}{\cosh(a_n t)} \qquad n = 1-3 \tag{55}$$

with b_n and a_n real and $a_n > b_n$. There is no special significance to this form, although it is even in t (as required) and is flexible enough to decay to zero with two different time scales (as is often found experimentally[2,3] and in computer simulation[4,5,7,42−44]). This functional form (although sometimes with b_n pure imaginary) has been useful in studies of both solvation dynamics[43,44] and vibrational energy relaxation.[45−49] Each correlation function can be characterized by the correlation time

$$\tau_n = \int_0^\infty \mathrm{d}t\, C_n(t)/C_n(0) = \frac{\pi}{2a_n}\sec(b_n\pi/2a_n) \tag{56}$$

Let us first simply consider the absorption spectrum, given by eq 9, which depends only on $C_1(t)$ (through $g_1(t)$). For the sake of definiteness, we take $b_1 = 0.556$ ps^{-1} and $a_1 = 2.63$ ps^{-1}, which gives $\tau_1 = 0.63$ ps. We consider three different values of σ_1: (A) 1.09 ps^{-1}, (B) 6.18 ps^{-1}, (C) 15.6 ps^{-1}, which gives $\sigma_1\tau_1 = 0.69$, 3.9, and 9.9, respectively. In Figure 2 are shown the calculated spectra for the three cases. For comparison we also show the distribution of frequencies

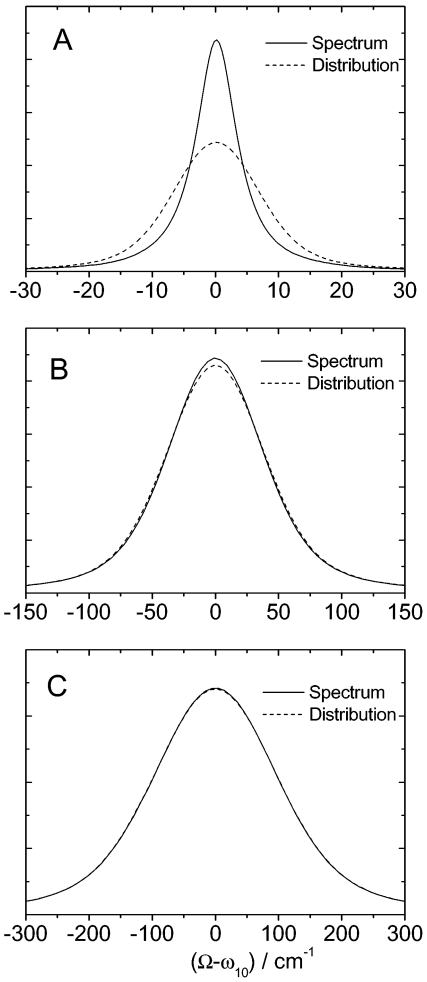

Figure 2. Absorption spectrum (solid lines) from eq 9 and frequency distribution (dashed lines) from eq 57 for models A−C.

$$I(\Omega) = \frac{1}{\sqrt{2\pi}\sigma_1}\exp\left[-\frac{(\Omega-\omega_{10})^2}{2\sigma_1^2}\right] \tag{57}$$

which is identical to the absorption spectrum in the inhomogeneous limit (and which can be obtained from eq 9 simply by replacing $C_1(t)$ by $C_1(0) = \sigma_1^2$). We see that in case A there is significant motional narrowing (the spectrum is narrower than the distribution of frequencies), as expected because $\sigma_1\tau_1 < 1$. Case B shows only a very small amount of motional narrowing, and case C shows none at all (again, as expected, because here $\sigma_1\tau_1 \gg 1$).

Next we turn our attention to the (integrated) 3PE intensity in the case when the three VSCFs are equal (as discussed in section III.C), and so accordingly we take $C_2(t) = C_3(t) = C_1(t)$, and $C_1(t)$ is given as above. We have seen that in the inhomogeneous ($\sigma_1\tau_1 \gg 1$) limit the normalized VSCF $\bar{C}_1(t_2)$ is equal to the normalized slope of the integrated intensity. Thus in panel 1 of Figure 3 we compare the normalized slope, from eqs 10, 14, and 25, with $\bar{C}_1(t_2)$, for each of the three models A−C. For the calculation of the normalized slope we used an anharmonicity of $\Delta = 2.45$ ps^{-1} (corresponding to 13 cm^{-1}). We see that for model C (the most inhomogeneous model) the agreement is quite good, whereas for models B and A it is less good. As noted above, one can improve upon these results when not in the inhomogeneous limit by using eqs 23 and 28 instead of eq 14 to approximate $\bar{C}_1(t_2)$. This is shown in panel 2 of Figure 3. One indeed sees significant improvement for models B and C, but in fact model A gets worse, evidently because for

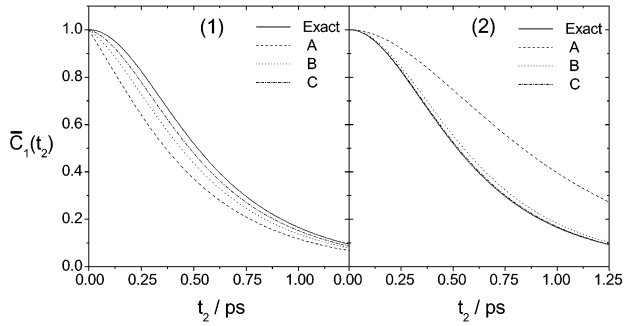

Figure 3. $\bar{C}_1(t_2)$ (solid lines in both panels), compared with integrated intensity slope results from eq 14 in panel 1 and eq 23 in panel 2, for models A−C.

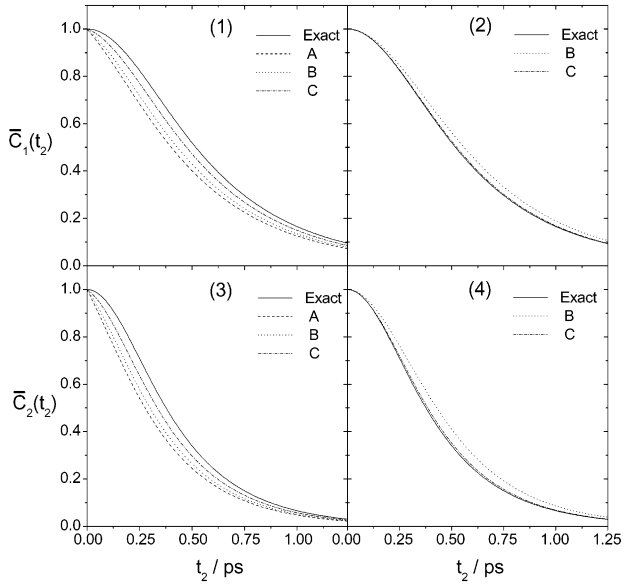

Figure 4. Panels 1 and 2: $\bar{C}_1(t_2)$ (solid lines in both panels), compared with heterodyned amplitude slope results from eq 40 in panel 1, and eq 36 in panel 2, for models A−C. Panels 3 and 4: $\bar{C}_2(t_2)$ (solid lines in both panels), compared with heterodyned amplitude slope results from eq 40 in panel 3, and eq 37 in panel 4, for models A−C.

this small value of $\sigma_1\tau_1$ the perturbation approach used to derive eq 23 breaks down.

When the anharmonicity is not as weak, the three VSCFs can be different. Because here we are trying mainly to resolve the difference between $C_1(t)$ and $C_2(t)$, to study this case numerically, we take $a_1 = a_3 = 2.63$ ps^{-1}, $b_1 = b_3 = 0.556$ ps^{-1}, $a_2 = 3.57$ ps^{-1}, and $b_2 = 0.588$ ps^{-1}. These parameters give $\tau_1 = \tau_3 = 0.63$ ps and $\tau_2 = 0.46$ ps. Thus in this model $C_2(t)$ decays significantly faster than $C_1(t)$. For simplicity we take $\sigma_1 = \sigma_2 = \sigma_3$, with the same three values as above, and we again take the anharmonicity to be $\Delta = 2.45$ ps^{-1} and $\kappa^2 = 2$. When the system is in the inhomogeneous limit, in section III.E we showed that one can obtain both $\bar{C}_1(t)$ and $\bar{C}_2(t)$ from the normalized slope of the half-Fourier transformed heterodyned amplitude evaluated at the frequencies ω_{21} and ω_{10}, respectively. Thus in panel 1 of Figure 4 we compare $\bar{C}_1(t_2)$ with results from eq 40, where the slope is defined in eq 33, the complex amplitude comes from eq 12, and the response function is given by eq 6. We see that although the results get progressively better going from model A to model C, even in the last case we are still not in quantitative agreement with $\bar{C}_1(t_2)$. In panel 2 is the better approximation from eqs 36 and 38. Here we see that the result for model C is in excellent agreement with $\bar{C}_1(t_2)$. There is no result shown for model A,

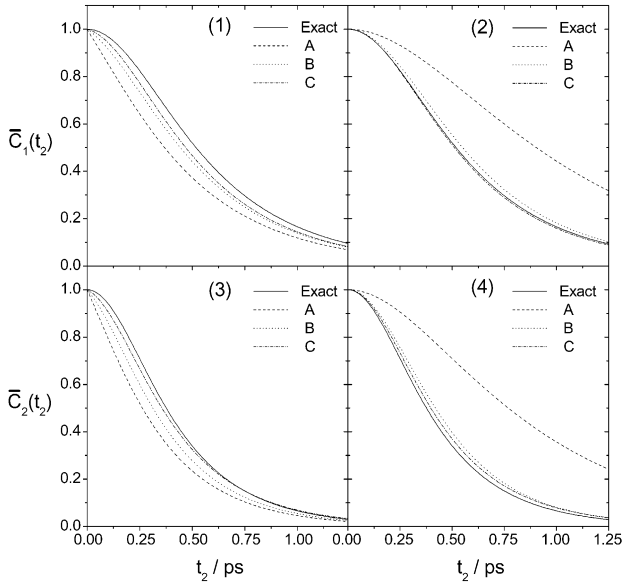

Figure 5. Panels 1 and 2: $\bar{C}_1(t_2)$ (solid lines in both panels), compared with frequency-dispersed intensity slope results from eq 51 in panel 1, and eq 49 in panel 2, for models A−C. Panels 3 and 4: $\bar{C}_2(t_2)$ (solid lines in both panels), compared with frequency-dispersed intensity slope results from eq 51 in panel 3, and eq 50 in panel 4, for models A−C.

because it turns out that for this small value of σ_1, T_1 is negative, again signaling a breakdown of perturbation theory. In panels 3 and 4 we compare $\bar{C}_2(t_2)$ with results from eq 40 and from eqs 37 and 39, and the results are similar. Note, however, that by comparing $\bar{C}_1(t_2)$ and $\bar{C}_2(t_2)$ in this figure one can clearly see the difference between them. The important point is that from evaluating the amplitude at the different frequencies, one can indeed discriminate between the two VSCFs, even when the two resonances overlap strongly.

When the resonances are separated, as shown in section III.F, one can use the F3PE intensity to determine the VSCFs. To demonstrate this, we take the same parameters as above, except now $\Delta = 56.5$ ps^{-1}, which is large compared to σ_1 even in model C. In Figure 5, panels 1 and 2, we compare $\bar{C}_1(t_2)$ to the results from eqs 51 and 49. The slope is calculated from eq 48, and the frequency-dispersed intensity comes from eqs 6, 12, and 13. Again we see that the results involving corrections to the slope are very good as the inhomogeneous limit is approached. Similar results are obtained for $\bar{C}_2(t_2)$ in panels 3 and 4, using eqs 51 and 50.

The general conclusion is that the proposed methods for determining the VSCFs involving the initial slopes of the integrated intensity, the heterodyned half-Fourier transformed amplitude, and the frequency-dispersed intensity, are all reasonably accurate as long as the dimensionless parameter $\sigma_1\tau_1 > 10$ (that is, the line shape is inhomogeneous). We also have shown that for systems with small amounts of motional narrowing ($\sigma_1\tau_1 > 5$) one can still obtain reasonably accurate results for the VSCFs by using our results that take into account first-order corrections. We believe that these methods can easily discriminate between VSCFs with correlation times τ_1 and τ_2 that differ by on the order of 10%.

V. How Correlated Are the 1−0 and 2−1 Frequencies?

The main point of this paper is to propose methods for determining VSCFs from different variants of vibrational three-pulse photon echo experiments and, in particular, to try to discriminate among the different VSCFs if indeed there are differences among them. It therefore behooves us to discuss

when there might or might not be differences. To this end we consider the fully microscopic Hamiltonian of an anharmonic oscillator coupled to an arbitrary bath:[50,51]

$$H = H_s + H_b + V \tag{58}$$

The oscillator and bath Hamiltonians are given by H_s and H_b, respectively, and V is the coupling. In a semiclassical approximation, where the oscillator is treated quantum mechanically and the bath is treated classically, the Hamiltonian for the oscillator in contact with the bath becomes time-dependent and is given by

$$H(t) = H_s + V(t) \tag{59}$$

Thus the coupling picks up the classical time dependence of the bath.

Defining $\delta V(t) = V(t) - \langle V \rangle$, we have

$$H(t) = H_s' + \delta V(t) \tag{60}$$

where $H_s' = H_s + \langle V \rangle$. H_s', the bath-renormalized oscillator Hamiltonian, has a set of eigenstates $|n\rangle$ with eigenvalues $\hbar\omega_n$. $H(t)$ can be expressed in this basis, and neglecting off-diagonal elements it becomes eq 1, where $\hbar\delta\omega_n(t) = (\delta V)_{nn}(t)$.

One can expand $V(t)$ in powers of the oscillator's coordinate q:[52]

$$V(t) = F(t)q + G(t)q^2 + ... \tag{61}$$

$F(t)$ and $G(t)$ are classical time-dependent bath variables. Therefore one can write

$$\hbar\delta\omega_n(t) = q_{nn}\delta F(t) + (q^2)_{nn}\delta G(t) + ... \tag{62}$$

where $\delta F(t) = F(t) - \langle F \rangle$ and $\delta G(t) = G(t) - \langle G \rangle$. The relevant VSCFs can therefore be written as

$$\begin{aligned} C_1(t) &= Q_{10}{}^2 C_{FF}(t) + 2Q_{10}P_{10}C_{FG}(t) + P_{10}{}^2 C_{GG}(t) \\ C_2(t) &= Q_{10}Q_{21}C_{FF}(t) + (Q_{10}P_{21} + Q_{21}P_{10})C_{FG}(t) \\ &\quad + P_{10}P_{21}C_{GG}(t) \\ C_3(t) &= Q_{21}{}^2 C_{FF}(t) + 2Q_{21}P_{21}C_{FG}(t) + P_{21}{}^2 C_{GG}(t) \end{aligned} \tag{63}$$

where $Q_{nm} \equiv (q_{nn} - q_{mm})/\hbar$, and $P_{nm} \equiv [(q^2)_{nn} - (q^2)_{mm}]/\hbar$. In the above

$$\begin{aligned} C_{FF}(t) &= \langle \delta F(t)\, \delta F(0) \rangle \\ C_{FG}(t) &= \langle \delta F(t)\, \delta G(0) \rangle \\ C_{GG}(t) &= \langle \delta G(t)\, \delta G(0) \rangle \end{aligned} \tag{64}$$

Now first suppose the oscillator is harmonic. In this case $q_{nn} = Q_{nm} = 0$ and $P_{10} = P_{21}$. This means that only the G fluctuations contribute, $\delta\omega_{21}(t) = \delta\omega_{10}(t)$, and in fact all three VSCFs are identical. Note this is only true if the expansion of V is truncated after third order, but this is generally an excellent approximation! Next suppose the oscillator is strongly anharmonic. In this case the diagonal matrix elements of q are nonzero, but still generally quite small. Nonetheless, the frequency fluctuations can still be dominated by the fluctuations in F (simply because the first-order term in the expansion is much larger) if the oscillator is anharmonic enough. In this case all VSCFs are proportional to $C_{FF}(t)$. Thus although the initial values σ_n will in general be different, the normalized VSCFs will be identical. In the situation intermediate between these two extremes, in general the initial values will all be different, as will the normalized VSCFs. The extent of the differences will of course depend on the parameters of the oscillator as well as on the microscopic model of the coupling and the bath.

VI. Concluding Remarks

In this paper we have explored methods for determining the vibrational solvation-correlation functions from three-pulse vibrational photon echo experiments. We have considered the integrated intensity, the heterodyned amplitude (actually its half-Fourier transform), and the frequency-dispersed intensity, and different specifications of the fluctuating anharmonic oscillator. In each of several cases we show that if the line shape is inhomogeneously broadened, or has only a small amount of motional narrowing, by defining a suitable initial slope in the t_1 direction, one can very simply determine the vibrational-correlation function for the fluctuations of the fundamental frequency, as well as the cross-correlation function for this fundamental frequency and the 2−1 frequency. We have also shown how peak-shift approaches can be used to determine the VSCFs at long time, just as in the case of electronic echoes.

Before we conclude, we must point out some possible problems with the approaches discussed herein. First of all, all the results described in this paper implicitly rest on the assumption that the frequency fluctuations can be treated classically. For typical vibrations in room-temperature liquids this should be a good approximation, because in this instance kT is greater than the width of the frequency fluctuations. Second, we have assumed that the cumulant truncation at second order is exact. This will of course only be true if the frequency fluctuations are Gaussian. Although much of the theoretical underpinning of condensed phase spectroscopy rests on this assumption,[38] and computer simulations for some models show that at least it is a reasonable approximation,[44,46] it remains to be seen how generally valid the assumption really is. Third, the slope approaches suffer from the same possible problems as in the electronic case (and perhaps even more so because of the longer IR pulses), which have to do with the effects of finite pulse convolutions[14,15,53] and pulse-ordering discontinuities.[40,41] Again, it remains to be seen how serious these problems are. Covering our bases, we have also discussed peak-shift approaches, for which the pulse-convolution problem may well be less serious, but of course these approaches have the disadvantage that they do not lead to short-time dynamics. Finally, all of these approaches rely to some extent on inhomogeneous broadening. Although for some systems like water this is clearly the case,[54,55] and for others like nitrogen it is clearly not,[52,56,57] most vibrations in simple liquids are probably somewhere between these two extremes, in the intermediate modulation regime. Despite these remarks of caution, we hope and expect that the approaches proposed herein will be useful in understanding dynamics in liquids using time-domain vibrational spectroscopy.

Acknowledgment. We are grateful for support from the National Science Foundation, grant nos. CHE-9816235 and CHE-0132538.

Appendix

In this Appendix we show how to evaluate some of the definite integrals that arise in the derivations of the results. We begin by defining the generating function

$$G(z) = \int_0^\infty dx\, e^{-x^2} e^{ixz} \tag{65}$$

Clearly

$$(-i)^n \frac{\mathrm{d}^n G(z)}{\mathrm{d}z^n} = \int_0^\infty \mathrm{d}x\, \mathrm{e}^{-x^2} x^n \mathrm{e}^{ixz} \tag{66}$$

$G(z)$ can be expressed in terms of Dawson's integral,

$$D(z) = \mathrm{e}^{-z^2} \int_0^z \mathrm{d}x\, \mathrm{e}^{x^2} \tag{67}$$

by[58,59]

$$G(z) = \frac{\sqrt{\pi}}{2} \mathrm{e}^{-z^2/4} + iD(z/2) \tag{68}$$

From the above it follows that

$$\int_0^\infty \mathrm{d}x\, \mathrm{e}^{-x^2} \cos(zx) = \frac{\sqrt{\pi}}{2} \mathrm{e}^{-z^2/4} \tag{69}$$

$$\int_0^\infty \mathrm{d}x\, \mathrm{e}^{-x^2} \sin(zx) = D(z/2) \tag{70}$$

$$\int_0^\infty \mathrm{d}x\, \mathrm{e}^{-x^2} x \cos(zx) = \frac{1}{2}[1 - zD(z/2)] \tag{71}$$

$$\int_0^\infty \mathrm{d}x\, \mathrm{e}^{-x^2} x \sin(zx) = \frac{z\sqrt{\pi}}{4} \mathrm{e}^{-z^2/4} \tag{72}$$

$$\int_0^\infty \mathrm{d}x\, \mathrm{e}^{-x^2} x^2 \cos(zx) = \frac{\sqrt{\pi}}{4}\left[1 - \frac{z^2}{2}\right] \mathrm{e}^{-z^2/4} \tag{73}$$

$$\int_0^\infty \mathrm{d}x\, \mathrm{e}^{-x^2} x^2 \sin(zx) = \frac{1}{2}\left\{\frac{z}{2} + \left[1 - \frac{z^2}{2}\right] D(z/2)\right\} \tag{74}$$

References and Notes

(1) Fleming, G. R.; Cho, M. *Annu. Rev. Phys. Chem.* **1996**, *47*, 109.
(2) Reynolds, L.; Gardecki, J. A.; Frankland, S. J. V.; Horng, M. L.; Maroncelli, M. *J. Phys. Chem.* **1996**, *100*, 10337.
(3) Horng, M. L.; Gardecki, J. A.; Papazyan, A.; Maroncelli, M. *J. Phys. Chem.* **1995**, *99*, 17311−17337.
(4) Stratt, R. M.; Maroncelli, M. *J. Phys. Chem.* **1996**, *100*, 12981.
(5) Bagchi, B.; Biswas, R. *Adv. Chem. Phys.* **1999**, *109*, 207.
(6) Saven, J. G.; Skinner, J. L. *J. Chem. Phys.* **1993**, *99*, 4391.
(7) Stephens, M. D.; Saven, J. G.; Skinner, J. L. *J. Chem. Phys.* **1997**, *106*, 2129.
(8) Ma, J.; Bout, D. V.; Berg, M. *J. Chem. Phys.* **1995**, *103*, 9146−9160.
(9) de Boeij, W. P.; Pshenichnikov, M. S.; Wiersma, D. A. *Annu. Rev. Phys. Chem.* **1998**, *49*, 99.
(10) Larsen, D. S.; Ohta, K.; Xu, Q.-H.; Cyrier, M.; Fleming, G. R. *J. Chem. Phys.* **2001**, *114*, 8008.
(11) de Boeij, W. P.; Pshenichnikov, M. S.; Wiersma, D. A. *Chem. Phys. Lett.* **1996**, *253*, 53.
(12) Cho, M.; Yu, J.-Y.; Joo, T.; Nagasawa, Y.; Passino, S. A.; Fleming, G. R. *J. Phys. Chem.* **1996**, *100*, 11944.
(13) Everitt, K. F.; Geva, E.; Skinner, J. L. *J. Chem. Phys.* **2001**, *114*, 1326.
(14) deBoeij, W. P.; Pshenichnikov, M. S.; Wiersma, D. A. *J. Phys. Chem.* **1996**, *100*, 11806.
(15) Joo, T.; Jia, Y.; Yu, J.; Lang, M. J.; Fleming, G. R. *J. Chem. Phys.* **1996**, *104*, 6089.
(16) Larsen, D. S.; Ohta, K.; Fleming, G. R. *J. Chem. Phys.* **1999**, *111*, 8970.
(17) Hamm, P.; Lim, M.; Hochstrasser, R. M. *Phys. Rev. Lett.* **1998**, *81*, 5326.
(18) Lim, M.; Hamm, P.; Hochstrasser, R. M. *Proc. Natl. Acad. Sci. U.S.A.* **1998**, *95*, 15315.
(19) Asplund, M. C.; Zanni, M. T.; Hochstrasser, R. M. *Proc. Natl. Acad. Sci. U.S.A.* **2000**, *97*, 8219.
(20) Zanni, M. T.; Asplund, M. C.; Hochstrasser, R. M. *J. Chem. Phys.* **2001**, *114*, 4579.
(21) Hamm, P.; Hochstrasser, R. M. In *Ultrafast Infrared and Raman Spectroscopy*; Fayer, M. D., Ed.; Markel Dekker: New York, 2001; p 273.
(22) Rella, C. W.; Rector, K. D.; Kwok, A.; Hill, J. R.; Schwettman, H. A.; Dlott, D. D.; Fayer, M. D. *J. Phys. Chem.* **1996**, *100*, 15620.
(23) Rector, K. D.; Thompson, D. E.; Merchant, K.; Fayer, M. D. *Chem. Phys. Lett.* **2000**, *316*, 122.
(24) Golonzka, O.; Khalil, M.; Demirdöven, N.; Tokmakoff, A. *Phys. Rev. Lett.* **2001**, *86*, 2154.
(25) Merchant, K. A.; Thompson, D. E.; Fayer, M. D. *Phys. Rev. Lett.* **2001**, *86*, 3899.
(26) Mukamel, S. *Annu. Rev. Phys. Chem.* **2000**, *51*, 691.
(27) Piryatinski, A.; Treiak, S.; Chernyak, V.; Mukamel, S. *J. Raman Spectrosc.* **2000**, *31*, 125.
(28) Piryatinski, A.; Chernyak, V.; Mukamel, S. In *Ultrafast Infrared and Raman Spectroscopy*; Fayer, M. D., Ed.; Markel Dekker: New York, 2001; p 349.
(29) Piryatinski, A.; Chernyak, V.; Mukamel, S. *Chem. Phys.* **2001**, *266*, 285.
(30) Thompson, D. E.; Merchant, K. A.; Fayer, M. D. *J. Chem. Phys.* **2001**, *115*, 317.
(31) Rector, K. D.; Jiang, J.; Berg, M. A.; Fayer, M. D. *J. Phys. Chem. B* **2001**, *105*, 1081.
(32) Berg, M.; vanden Bout, D. A. *Acc. Chem. Res.* **1997**, *30*, 65.
(33) Williams, R. B.; Loring, R. F.; Fayer, M. D. *J. Phys. Chem. B* **2001**, *105*, 4068.
(34) Stenger, J.; Madsen, D.; Hamm, P.; Nibbering, E. T. J.; Elsaesser, T. *Phys. Rev. Lett.* **2001**, *87*, 027401.
(35) Golonzka, O.; Khalil, M.; Demirdöven, N.; Tokmakoff, A. *J. Chem. Phys.* **2001**, *115*, 10814.
(36) Lim, M.; Hochstrasser, R. M. *J. Chem. Phys.* **2001**, *115*, 7629.
(37) Zanni, M. T.; Gnanakaran, S.; Stenger, J.; Hochstrasser, R. M. *J. Phys. Chem. B* **2001**, *114*, 4579.
(38) Mukamel, S. *Principles of Nonlinear Optical Spectroscopy*; Oxford: New York, 1995.
(39) Kubo, R. *Adv. Chem. Phys.* **1969**, *15*, 101.
(40) Hybl, J. D.; Faeder, S. M. G.; Albrecht, A. W.; Tolbert, C. A.; Green, D. C.; Jonas, D. M. *J. Lumin.* **2000**, *87−89*, 126.
(41) Faeder, S. M. G.; Jonas, D. M. *Phys. Rev. A* **2000**, *62*, 033820.
(42) Fonseca, T.; Ladanyi, B. M. *J. Mol. Liq.* **1994**, *60*, 1.
(43) Egorov, S. A.; Stephens, M. D.; Skinner, J. L. *J. Chem. Phys.* **1997**, *107*, 10485.
(44) Everitt, K. F.; Skinner, J. L. *Chem. Phys.* **2001**, *266*, 197.
(45) Egorov, S. A.; Skinner, J. L. *J. Chem. Phys.* **1996**, *105*, 7047.
(46) Everitt, K. F.; Egorov, S. A.; Skinner, J. L. *Chem. Phys.* **1998**, *235*, 115.
(47) Rabani, E.; Reichman, D. R. *J. Phys. Chem. B* **2001**, *105*, 6550.
(48) Poulsen, J. A.; Rossky, P. J. *J. Chem. Phys.* **2001**, *115*, 8014.
(49) Poulsen, J. A.; Rossky, P. J. *J. Chem. Phys.* **2001**, *115*, 8024.
(50) Oxtoby, D. W. *Adv. Chem. Phys.* **1979**, *40*, 1.
(51) Oxtoby, D. W. *Adv. Chem. Phys.* **1981**, *47 (Part 2)*, 487.
(52) Oxtoby, D. W.; Levesque, D.; Weis, J.-J. *J. Chem. Phys.* **1978**, *68*, 5528.
(53) Passino, S. A.; Nagasawa, Y.; Joo, T.; Fleming, G. R. In *Ultrafast Phenomena X*; Barbara, P. F., Fujimoto, J. G., Knox, W. H., Zinth, W., Eds.; Vol. 62 of Springer Series in Chemical Physics; Springer: Berlin, 1996; p 199.
(54) Gale, G. M.; Gallot, G.; Hache, F.; Lascoux, N.; Bratos, S.; Leicknam, J.-C. *Phys. Rev. Lett.* **1999**, *82*, 1068.
(55) Laenen, R.; Rauscher, C.; Laubereau, A. *Phys. Rev. Lett.* **1998**, *80*, 2622.
(56) Gayathri, N.; Bagchi, B. *J. Phys. Chem. A* **1999**, *103*, 9579.
(57) Everitt, K. F.; Skinner, J. L. *J. Chem. Phys.* **2001**, *115*, 8531.
(58) Abramowitz, M.; Stegun, I. A. *Handbook of Mathematical Functions*; Dover: New York, 1972.
(59) Gradshteyn, I. S.; Ryzhik, I. M. *Table of Integrals, Series and Products*; Academic Press: New York, 1965.